VOYAGER 1 NEAR THE HELIOPAUSE

S. N. BOROVIKOV[1] AND N. V. POGORELOV[1,2]
[1] Center for Space Physics and Aeronomic Research, The University of Alabama in Huntsville,
Huntsville, AL 35805, USA; nikolai.pogorelov@uah.edu
[2] Department of Space Sciences, The University of Alabama in Huntsville, Huntsville, AL 35805, USA

ABSTRACT

Recent observations from the *Voyager 1* spacecraft show that it is sampling the local interstellar medium (LISM). This is quite surprising because no realistic, steady-state model of the solar wind (SW) interaction with the LISM gives an inner heliosheath width as narrow as ∼30 AU. This includes models that assume a strong redistribution of the ion energy to the tails in the pickup ion distribution function. We show that the heliopause (HP), which separates the SW from the LISM, is not a smooth tangential discontinuity, but rather a surface subject to Rayleigh–Taylor-type instabilities which can result in LISM material penetration deep inside the SW. We also show that the HP flanks are always subject to a Kelvin–Helmholtz instability. The instabilities are considerably suppressed near the HP nose by the heliospheric magnetic field in steady-state models, but reveal themselves in the presence of solar cycle effects. We argue that *Voyager 1* may be in one such instability region and is therefore observing plasma densities much higher than those in the pristine SW. These results may explain the early penetration of *Voyager 1* into the LISM. They also show that there is a possibility that the spacecraft may start sampling the SW again before it finally leaves the heliosphere.

Key words: ISM: kinematics and dynamics – ISM: magnetic fields – solar wind – Sun: heliosphere

Online-only material: animation, color figures

1. INTRODUCTION

On 2012 August 25, *Voyager 1* (hereafter *V1*) measured the third in a series of three sudden drops in the intensity of low energy ions it had been observing for the previous 6 yr, and those ions virtually disappeared (Krimigis et al. 2013; Stone et al. 2013). At the same time, the intensity of cosmic-ray electrons (>70 MeV) and protons from the heliospheric exterior abruptly increased (see a detailed discussion in Webber et al. 2013). The simplest explanation for these observations could be the penetration of *V1* into the local interstellar medium (LISM). On the other hand, observations from the *V1* magnetometer indicated no substantial changes in the heliospheric magnetic field (HMF) direction (Burlaga et al. 2013a, 2013b) during that latest drop. The magnetic field vector elevation and azimuthal angles remained close, but not exactly equal, to the Parker spiral direction (the differences being $14°$ and $17°$, respectively). Additionally, numerical models taking into account solar-cycle variations in the solar wind (SW) consistently showed a substantial increase in the radial and latitudinal components of the HMF at different stages of the solar cycle (Pogorelov et al. 2009a, 2013a, 2013b). The magnetic field behavior across the heliopause (HP), of course, depends on the direction of the interstellar magnetic field (ISMF), as seen from the simulations of Pogorelov et al. (2004, 2006, 2011). *Solar Heliospheric Observatory* (*SOHO*) measurements of the Lyα backscattered emission (Lallement et al. 2005) and an *Interstellar Boundary Explorer* (*IBEX*) discovery (McComas et al. 2009) of a bright and spatially narrow enhancement in the energetic neutral atom (ENA) fluxes (the so-called *IBEX* ribbon) made it possible to impose certain restrictions on the ISMF direction and strength (Heerikhuisen et al. 2010; Heerikhuisen & Pogorelov 2011; Pogorelov et al. 2008, 2009b). This allowed Heerikhuisen et al. (2010) to reproduce the ribbon with remarkable accuracy. Pogorelov et al. (2009c), Borovikov et al. (2011), Ratkiewicz et al. (2012) used those

restrictions to validate their simulations results. The choice of the *BV* plane, a plane formed by the velocity and magnetic field vectors in the unperturbed LISM, is especially important for reproducing the ribbon. Solar cycle simulations in Pogorelov et al. (2009a, 2012a, 2013b) were successful in reproducing one of the recent puzzles related to the *V1* observation of the negative radial velocity component (Krimigis et al. 2011; Decker et al. 2012) and suggested that there may exist substantially different inner heliosheath (IHS) regions separated by time-dependent magnetic barriers.

As reported by Gurnett et al. (2013), the *V1* plasma wave instrument measured the electron density from the frequency of electron plasma oscillations. The densities measured were in the range of 0.06 to 0.08 cm^{-3} and are large for the SW. Although it is clear that *V1* is in the LISM plasma, two questions remain unanswered: (1) why was there no substantial change in the magnetic field direction observed and (2) why did the heliocentric distance of the HP in the *V1* direction turn out to be so small (∼121 AU)? The first question is somewhat simpler because the magnetic field behavior on the outer side of the HP may be affected by different processes, including those described below. In principle, as seen from the solar cycle simulations by Pogorelov et al. (2009a, 2013b), the **B** elevation and azimuthal angles behind the HP are varying near average values of $25°$ and $190°$, respectively, which agrees with Burlaga & Ness (2014). Another possibility based on an analogy with magnetic flux transfer events in the Earth's magnetosphere was proposed by Schwadron & McComas (2013). Our simulations based on exact fitting of the HP do not confirm the idea of Opher & Drake (2013) that the ISMF vector becomes nearly parallel to the solar equatorial plane regardless of its direction in the unperturbed LISM, presumably due to the plasma diffusion. As estimated by Fahr et al. (1986) in a detailed review of the physical processes that result in the mixing of the SW and LISM plasma at the HP, the width of the HP based

solely on diffusion processes should be smaller than 0.01 AU, with diffusion velocities of about 10^{-6} of the Alfvén velocity. However, considerably larger mixing distances are possible in the presence of magnetic reconnection and hydrodynamic instabilities (see Fahr & Neutsch 1983a, 1983b), which makes the plasma interpenetration "spotty," as seen in our results presented below.

The second question is especially challenging since the observed asymmetries in the heliospheric termination shock (TS) required considerably larger HP distances from the Sun in the *V1* direction compared with the *Voyager 2* (hereafter *V2*) direction (Pogorelov et al. 2004; Opher et al. 2006). ISMF directions agreeable with the *IBEX* ribbon also give an IHS width of about 50–60 AU (Borovikov et al. 2011; Heerikhuisen et al. 2008). It is clear that one must remove the plasma energy from the IHS to make it narrower. This process is intrinsic to the IHS plasma flow because of its charge exchange with the interstellar neutral atoms (see, e.g., Baranov & Malama 1993; Pauls et al. 1995; Zank et al. 1996). This is especially true for pickup ions, the pressure of which is dominant in the IHS. Charge exchange in this case gives birth to ENAs which are later observed by *IBEX*. Heerikhuisen et al. (2008) proposed to make the energy withdrawal more realistic by assuming a Lorentzian (kappa) distribution of ions in the IHS. This made it possible to decrease the IHS width in the *V1* direction to $\sim$50 AU (for $\kappa = 1.63$), but this is insufficient to account for the *V1* crossing at $\sim$121 AU, and other reasons should be sought.

The HP can hardly be expected to be a smooth classical MHD tangential discontinuity. The internal structure of tangential discontinuities in collisionless plasma has not been investigated in detail yet and naturally requires 3D full-particle and/or hybrid simulations. The HP may be also subject to magnetic reconnection between the HMF and ISMF, and possibly hydrodynamic instabilities. Ruderman & Fahr (1995) considered the HP nose instability as a shear-flow instability of the Kelvin–Helmholtz type. Chalov (1996) investigated the stabilizing effect of the HP curvature. Ruderman & Belov (2010) showed that this instability should rather be classified as a negative-energy instability. The Rayleigh–Taylor instability of the HP, attributed to charge exchange by Liewer et al. (1996) and Zank et al. (1996), and Zank (1999) was considered numerically by Florinski et al. (2005) and Borovikov et al. (2008) assuming an axially symmetric configuration of the SW–LISM interaction, which requires the absence of the HMF and the assumption that the LISM velocity and ISMF vectors are parallel to each other. The latter assumption results in the ISMF vanishing at the LISM stagnation point on the HP and ensures a relatively weak ISMF when *V1* crosses the HP. Being a tangential discontinuity, the HP is unconditionally unstable in the absence of surface tension (e.g., due to magnetic fields). Magnetic field tension can stabilize the HP in the absence of charge exchange. Charge exchange and magnetic field tension compete with each other. Three-dimensional, steady-state simulations, even those performed with extremely high resolution near the HP ($\sim$0.02 AU), showed no signs of instability at the HP nose (Borovikov et al. 2011).

The aim of this Letter is to demonstrate that the HP can be unstable in a situation involving solar cycle effects. The HMF can be substantially depressed at the nose of the HP near solar maxima. This creates an instability that, when looked at in the meridional plane, slowly moves to higher latitudes until it reaches the *V1* location. In this way, spacecraft observations may be reconciled with the theoretical heliocentric

Table 1
The SW Parameters, Scaled to 1 AU, Used as
Initial Boundary Conditions in Model (d)

Quantity	Slow SW	Fast SW
Number density, n, cm^{-3}	6.9	2.4
Radial velocity component, V, km s^{-1}	450	762
Temperature, **T**, K	68000	245000
Radial component of the HMF, **B$_R$**, nT	3.5	3.5

distance where *V1* crossed the HP and penetrated into the LISM.

2. HP INSTABILITIES

We performed simulations using the LISM flow parameters from McComas et al. (2012), where the presence of a bow shock in the LISM plasma ahead of the HP was investigated (plasma density 0.082 cm^{-3}, velocity 23.2 km s^{-1}, and temperature 6300 K). The ISMF strength in the unperturbed LISM is $B_\infty = 0.3$ nT and the neutral hydrogen density is 0.172 cm^{-3}. Its direction is specified by the vector $\mathbf{l}_{B_\infty} = (255°, 44°)$ in the ecliptic coordinates and chosen to fit the *IBEX* ribbon (Heerikhuisen et al. 2014). We used four different SW models, which are summarized below.

(a) A spherically symmetric SW with the following properties at 1 AU: the number density $n_E = 7.4$ cm^{-3}, radial velocity $v_E = 450$ km s^{-1}, and temperature $T_E = 5.1 \times 10^5$ K. The radial component B_R of the HMF at 1 AU is 3.75 nT. The tilt angle between the Sun's rotation and magnetic axes is zero.

(b) The same as (a), but no HMF. This model is similar to a 2D axially symmetric SW model accepted in the HP instability study by Borovikov et al. (2008).

(c) The same as (a), but no ISMF.

(d) A solar cycle model with the SW properties roughly corresponding to *Ulysses* measurements during the 23rd solar cycle (see Table 1) and LISM properties the same as in model (a).

The boundary between the fast and slow SW flows is determined by the latitudinal extent of the slow SW and assumed to be an 11 yr periodic function ensuring the change in the angular extent from 28° at solar minima to 90° at solar maxima. The angle between the Sun's rotation and magnetic axes is also assumed to be an 11 yr periodic function changing from 8° at solar minima to 90° at solar maxima. The HMF polarity changes to the opposite polarity every 11 yr at solar maxima. Simulations were performed on a mesh dynamically adapting to the HP and ensuring an effective resolution of about 0.2 AU in its vicinity.

The top left panel in Figure 1 shows the shape of the HP for model (a). The HP is identified exactly using a level-set method described in Borovikov et al. (2011). In all simulations we use a four-fluid model as described in Pogorelov et al. (2006). The top right and bottom panels of Figure 1 show the plasma density distributions (for models (a), (b), and (c), respectively) in the meridional plane, which is defined by the Sun's rotation axis and the velocity vector $\mathbf{V}_\infty$ in the unperturbed LISM. It is seen that the HP is unstable at its flanks, but no instability is seen at the nose for substantial HMF strength on the inner side of the HP. This remains true for model (c), where the ISMF is set to zero. A zero-tilt model (model (a)) results in a flat heliospheric current sheet (HCS) that bends northward on crossing the TS and creates a layer of strong unipolar magnetic field with the southern-hemisphere polarity on the inner surface of the HP. The reason is the ISMF pressure exerted on the HP. Artificially eliminating the ISMF does not destabilize the HP,
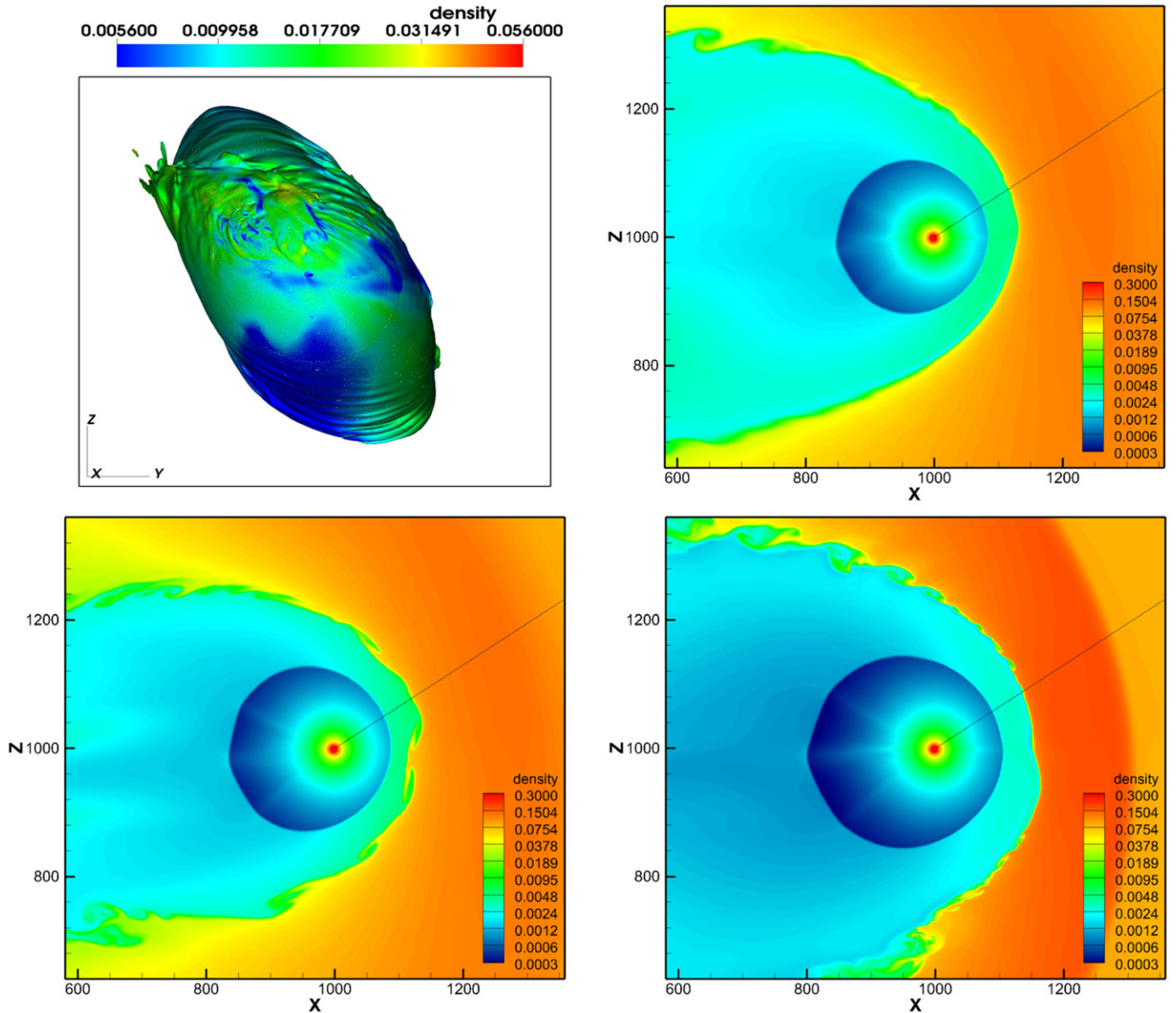
Figure 1. Top panel: frontal (LISM) view of the heliopause colored by plasma density values (left) and the distribution of plasma density in the meridional plane (right) for model (a) (both HMF and ISMF are taken into account). Bottom panel: plasma density distributions in the meridional plane for (left) model (b) (zero HMF, non-zero ISMF) and (right) model (c) (zero ISMF, non-zero HMF).

(A color version of this figure is available in the online journal.)

whereas the absence of the HMF produces a typical instability structure (see the bottom left panel in Figure 1), which allows the LISM plasma to penetrate into the IHS. The topology of the instability regions is different from those observed in the earlier axially symmetric models without HMF. For a realistic ISMF orientation, these regions appear to be aligned with the ISMF lines draping around the HP. This is seen in the top right panel of Figure 2.

As discussed in Borovikov et al. (2008), the HP flanks are unstable in the absence of magnetic fields because of the violent Kelvin–Helmholtz instability accompanying the shear flow regions along the HP separating the SW and LISM plasma. The HP nose becomes unstable due to the momentum exchange caused by the charge-exchange processes. The comparison of the first three models led us to two natural conclusions: (1) the HMF and ISMF tension is insufficient to stabilize the HP flanks and (2) the HP nose may be strongly destabilized during periods of small HMF.

Numerical solutions of the SW–LISM interaction which take into account solar cycle effects (Pogorelov et al. 2009a, 2012a, 2013b) show that the periods of small HMF are typical in the HP regions adjacent to the *V1* crossing point due to the turbulence that destroys the regular HCS structure when its injection scale is comparable with the width of the unipolar HMF regions (Lazarian & Opher 2009). The latter shrinks to zero as the SW plasma approaches the flow stagnation point on the inner side of the HP (see, e.g., Borovikov et al. 2011; Pogorelov et al. 2013b). The solar cycle effects are seen in Figure 2.

Raleigh–Taylor instability initially develops at the HP nose. It is seen as a fold aligned with the ISMF on the HP surface (the top left panel in Figure 2). The maximum penetration of the LISM inside the IHS occurs at the HP front, the penetration layer starts extending to higher latitudes, and passes through the *V1* trajectory. As in Borovikov et al. (2008), there is no single frequency in the instability development, but the interval between the deepest LISM penetrations into the IHS in the
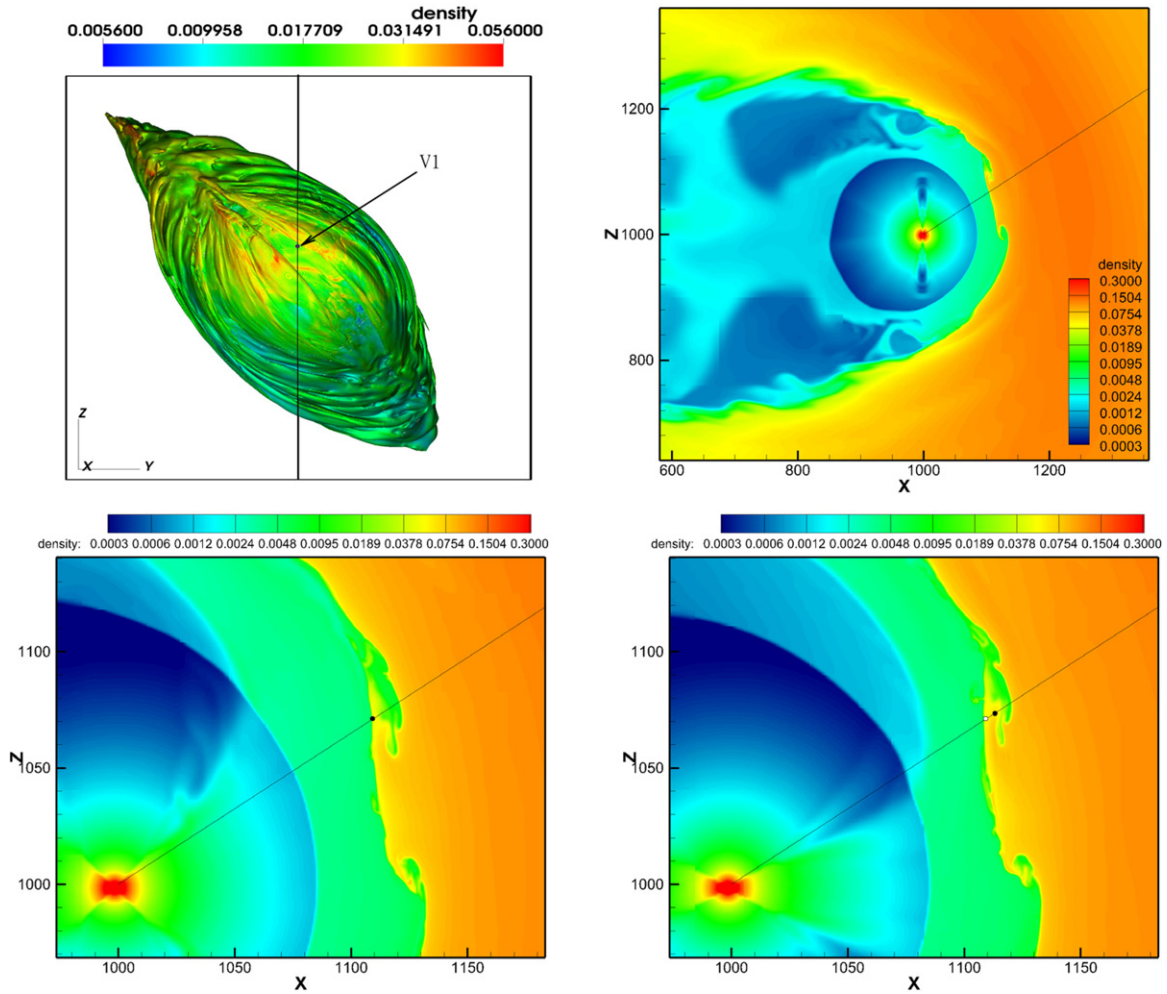
Figure 2. Top panel: heliopause colored by plasma density values (left) and distribution of plasma density in the meridional plane (right) for model (d). Bottom panel: possible scenario of *Voyager 1* moving through the instability. Left panel: initial crossing of the HP. Right panel: position of *V1* 2 yr later as the HP evolves.

(An animation and a color version of this figure are available in the online journal.)

equatorial plane is about 180 yr. Less deep penetrations occur more frequently (∼50 yr interval). The time evolution of the instability is shown in the animation available in the online journal. As the instability regions evolve in time and in space, they change their shape and size, and the penetration depth diminishes. However, strong penetration (up to ∼20 AU) of the LISM plasma into the IHS is typical, and there is a strong possibility that *V1* is in such a region now. In the meridional plane, the instability region is seen as a clump of the LISM plasma moving poleward. However, its 3D topology is more complicated. The two bottom panels in Figure 2 show the plasma density distribution in the meridional plane. The points show the *V1* position at the moment it crosses the HP and two years afterward. Comparing the left and right panels, we see the evolution of the instability. There is a possibility that *V1* may penetrate the SW again. However, our solution shows that the magnetic field in this complex-shape SW region no longer resembles the Parker field.

The left panel of Figure 3 shows the plasma density distribution along the *V1* and *V2* trajectories. The black and blue lines (lines (a) and (b)) show the plasma density profiles along the *V1* direction at the moments of time shown in the top right and bottom left panels of Figure 2. Line *c* shows the same along the *V2* direction at the time shown in the top right panel of the same figure. One can see that the density at *V1* reaches the value of about

$0.065\ \mathrm{cm}^{-3}$ immediately after crossing, which is consistent with Gurnett et al. (2013), and continues increasing afterward (note the logarithmic scale of the figure). The TS is at ∼89 AU at the moment of crossing, while the HP itself is at 124 AU, which is also in reasonable agreement with *V1* observations. The density jump occurs within 1–2 AU, which is consistent with numerical smearing for the resolution of 0.2 AU. Note that Belov & Ruderman (2010) argued that charge exchange can eliminate jumps in plasma quantities across the HP at the stagnation point (in the absence of magnetic fields) and make the HP transition as wide as 5 AU.

It is interesting that the instantaneous density profiles are very similar in the *V1* and *V2* directions. Numerical simulations continued another solar cycle ahead show that the HP position in the *V2* direction is changing in the interval ±3 AU, which means that one can expect *V2* to cross the HP at a heliocentric distance of about 121–127 AU. This may happen in 5–7 yr.

The right panel of Figure 3 and the left panel of Figure 4 show, respectively, the distributions of the magnetic field components and the magnetic field elevation and azimuthal angles, δ and λ, along the instantaneous trajectory corresponding to line *a* on the left panel. We see that δ increases to 35° across the HP and continues increasing to 42°. At the same time λ becomes ∼281° and further increases to ∼285°. The angle changes across the HP are substantial and should be instantaneous in an ideal
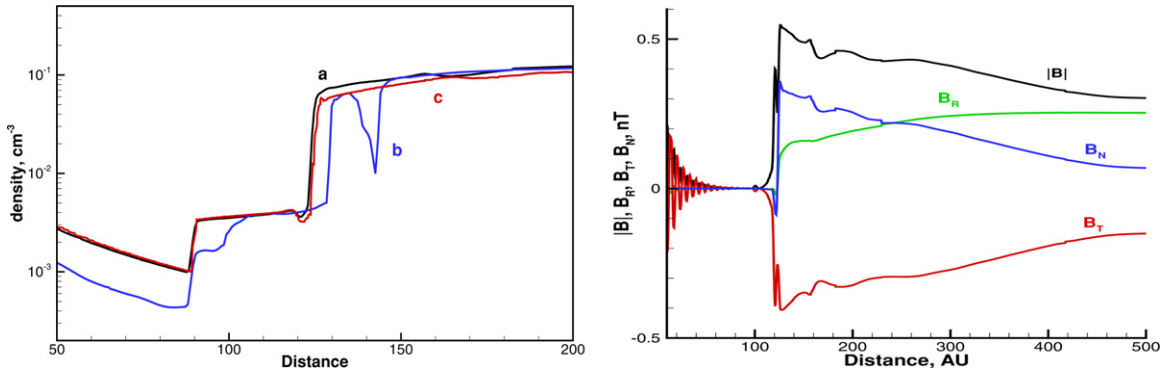
Figure 3. Left panel: instantaneous distributions of plasma density along the *V1* trajectory (black (a) and blue (b) lines correspond to the solutions shown in the top right and bottom left panels in Figure 2, respectively) and the *V2* trajectory (red (c) line corresponds to the top right panel of Figure 2). Right panel: instantaneous distributions of the magnetic field vector magnitude |**B**| and its *R*, *T*, and *N* components in the *V1* trajectory direction for the solution shown in the top right panel of Figure 2.

(A color version of this figure is available in the online journal.)
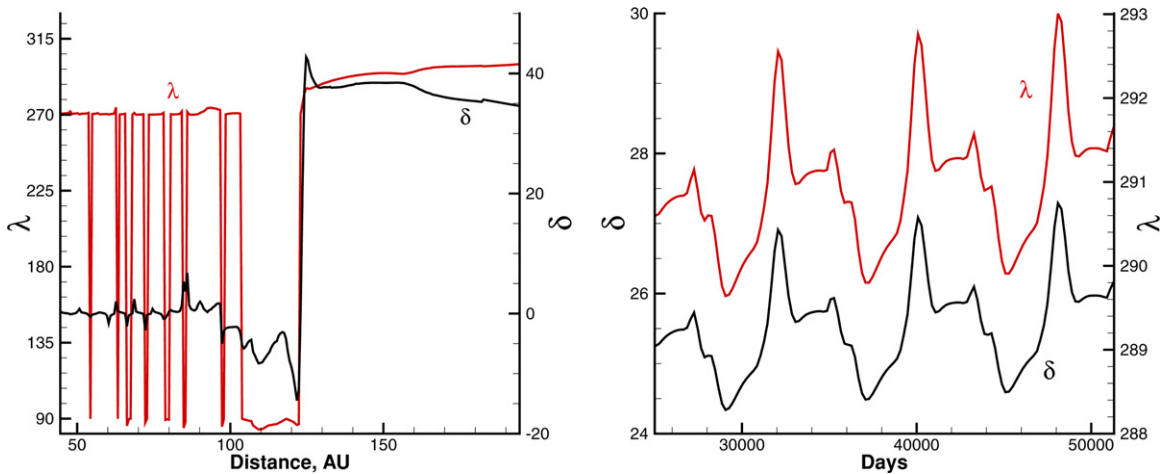
Figure 4. Left panel: instantaneous distributions of the **B** elevation and azimuthal angles (δ and λ) in the *V1* trajectory direction for the solution shown in the top right panel of Figure 2. Right panel: time variation of the **B** elevation and azimuthal angles behind the HP in the *V1* trajectory direction in the solar cycle model by Pogorelov et al. (2009a).

(A color version of this figure is available in the online journal.)

MHD model. However, numerical smearing obviously makes the transition gradual, though quite sharp. It is interesting that *V1* measured $\delta \approx 14°$ immediately after the HP crossing, but this angle increased to ~25° by the end of 2013 (Burlaga & Ness 2014).

3. CONCLUSION

We have shown that the solar cycle creates conditions favorable for HP instability and deep penetration of the LISM plasma into the IHS. The primary reason for the instability is charge exchange, but temporary decreases of the HMF strength at the *V1* latitude prevent the magnetic field tension from stabilizing the HP. As discussed by Fahr et al. (1986) and Ruderman & Fahr (1995), ram pressure variations related to the solar cycle may also contribute to the HP destabilization. However, our simulations show violent instabilities in the absence of HMF even for a steady, spherically symmetric SW. The changes in density across the HP are in agreement with *V1* observations. There is some discrepancy in the magnetic field deflection angles. Note that our previous solar cycle model (Pogorelov et al. 2009a), which used the LISM properties acceptable before the proposed modifications in the LISM velocity vector (McComas et al. 2012) and assumed a lower angle between the LISM velocity and ISMF vectors (30° versus 49° in the current

simulation), gives δ and λ in better agreement with observations (see Figure 4). This discrepancy, as well as the deviation of our new *BV* plane from the plane formed by the new He atom velocity direction and the H atom velocity vector measured in the inner heliosphere by Lallement et al. (2005), requires further analysis. Note that the *BV* planes in Pogorelov et al. (2009a); Heerikhuisen & Pogorelov (2011) and our current simulation are nearly parallel, which is reasonable because they were both chosen to fit the *IBEX* ribbon.

We have shown that the HP excursions in the direction of the *V2* trajectory are smaller than at *V1*. It is therefore likely that *V2* will cross the HP in 5–7 yr. Judging by the small distance between consecutive ACR decreases at *V1* during 2012 July–August, the spacecraft might have been crossing the fine structure of the instability. Penetration of the LISM plasma into the IHS may be responsible for the observed energetic ion behavior (Florinski et al. 2013).

REFERENCES

Baranov, V. B., & Malama, Y. G. 1993, JGR, 98, 15157
Belov, N. A., & Ruderman, M. S. 2010, MNRAS, 401, 607
Borovikov, S. N., Pogorelov, N. V., Burlaga, L. F., & Richardson, J. D. 2011, ApJL, 728, L21
Borovikov, S. N., Pogorelov, N. V., Zank, G. P., & Kryukov, I. A. 2008, ApJ, 682, 1404
Burlaga, L. F., & Ness, N. F. 2014, ApJL, in press
Burlaga, L. F., Ness, N. F., Gurnett, D. A., & Kurth, W. S. 2013a, ApJL, 778, L3
Burlaga, L. F., Ness, N. F., & Stone, E. C. 2013b, Sci, 341, 147
Chalov, S. V. 1996, A&A, 308, 995
Decker, R. B., Krimigis, S. M., Roelof, E. C., & Hill, M. E. 2012, Natur, 489, 124
Fahr, H. J., & Neutsch, W. 1983a, MNRAS, 205, 839
Fahr, H. J., & Neutsch, W. 1983b, A&A, 118, 57
Fahr, H. J., Neutsch, W., Grzedzielski, S., Macek, W., & Ratkiewicz-Landowska, R. 1986, SSRv, 43, 329
Florinski, V., Jokipii, J. R., Alouani-Bibi, F., & le Roux, J. A. 2013, ApJL, 776, L37
Florinski, V., Zank, G. P., & Pogorelov, N. V. 2005, JGR, 110, A07104
Gurnett, D. A., Kurth, W. S., Burlaga, L. F., & Ness, N. F. 2013, Sci, 341, 1489
Heerikhuisen, J., & Pogorelov, N. V. 2011, ApJ, 738, 29
Heerikhuisen, J., Pogorelov, N. V., Florinski, V., Zank, G. P., & le Roux, J. A. 2008, ApJ, 682, 679
Heerikhuisen, J., Pogorelov, N. V., Zank, G. P., et al. 2010, ApJL, 708, L126
Heerikhuisen, J., Zirnstein, E. J., Funsten, H. O., Pogorelov, N. V., & Zank, G. P. 2014, ApJ, in press
Krimigis, S. M., Decker, R. B., Roelof, E. C., et al. 2013, Sci, 341, 144
Krimigis, S. M., Roelof, E. C., Decker, R. B., & Hill, M. E. 2011, Natur, 474, 359
Lallement, R., Quémerais, E., Bertaux, J.-L., et al. 2005, Sci, 307, 1447
Lazarian, A., & Opher, M. 2009, ApJ, 703, 8
Liewer, P. C., Karmesin, S. R., & Brackbill, J. U. 1996, JGR, 101, 17119
McComas, D. J., Alexashov, D., Bzowski, M., et al. 2012, Sci, 336, 1291
McComas, D. J., Allegrini, F., Bochsler, P., et al. 2009, Sci, 326, 959
Opher, M., & Drake, J. 2013, ApJL, 778, L26
Opher, M., Stone, E. C., & Liewer, P. C. 2006, ApJL, 640, L71
Pauls, H. L., Zank, G. P., & Williams, L. L. 1995, JGR, 100, 21595
Pogorelov, N. V., Borovikov, S. N., Burlaga, L. F., et al. 2013a, in AIP Conf. Proc. 1539, Solar Wind 13, ed. P. Zank et al. (Melville, NY: AIP), 352
Pogorelov, N. V., Borovikov, S. N., Zank, G. P., & Ogino, T. 2009a, ApJ, 696, 1478
Pogorelov, N. V., Borovikov, S. N., Zank, G. P., et al. 2012a, ApJL, 750, L4
Pogorelov, N. V., Heerikhuisen, J., Mitchell, J. J., Cairns, I. H., & Zank, G. P. 2009b, ApJL, 695, L31
Pogorelov, N. V., Heerikhuisen, J., & Zank, G. P. 2008, ApJL, 675, L41
Pogorelov, N. V., Heerikhuisen, J., Zank, G. P., & Borovikov, S. N. 2009c, SSRv, 143, 31
Pogorelov, N. V., Heerikhuisen, J., Zank, G. P., et al. 2011, ApJ, 742, 104
Pogorelov, N. V., Suess, S. T., Borovikov, S. N., et al. 2013b, ApJ, 772, 2
Pogorelov, N. V., Zank, G. P., & Ogino, T. 2004, ApJ, 614, 1007
Pogorelov, N. V., Zank, G. P., & Ogino, T. 2006, ApJ, 644, 1299
Ratkiewicz, R., Strumik, M., & Grygorczuk, J. 2012, ApJ, 756, 3
Ruderman, M. S., & Belov, N. A. 2010, J. Phys. Conf. Ser., 216, 012016
Ruderman, M. S., & Fahr, H. J. 1995, A&A, 299, 258
Schwadron, N. A., & McComas, D. J. 2013, ApJL, 778, L33
Stone, E. C., Cummings, A. C., McDonald, F. B., et al. 2013, Sci, 341, 150
Webber, W. R., McDonald, F. B., Cummings, A. C., et al. 2013, GeoRL, 39, L06107
Zank, G. P. 1999, in AIP Conf. Ser. 471, Solar Wind 9, ed. S. R. Habbal et al. (Melville, NY: AIP), 783
Zank, G. P., Pauls, H. L., Williams, L. L., & Hall, D. T. 1996, JGR, 101, 21639